CNC Machine Tool Digital Twin Applications with Advancements of Edge Computing

by

Cemile Beşirova

A Dissertation Submitted to the
Graduate School of Sciences and Engineering
in Partial Fulfillment of the Requirements for
the Degree of

Master of Science

in

Mechanical Engineering

January, 2024

CNC Machine Tool Digital Twin Applications with Advancements of Edge Computing

Koç University

Graduate School of Sciences and Engineering

This is to certify that I have examined this copy of a master's thesis by

Cemile Beşirova

and have found that it is complete and satisfactory in all respects,

and that any and all revisions required by the final

examining committee have been made.

Committee Members:

Prof. İsmail Lazoğlu (Advisor)

Prof. Murat Sözer

Assoc. Prof. Ali Fuat Ergenç

Date: 16/01/2024

To my dear family and friends for your constant support...

ABSTRACT

CNC Machine Tool Digital Twin Applications with Advancements of Edge Computing

Cemile Beşirova

Master of Science in Mechanical Engineering

January 16, 2024

Digital Twin application development for CNC machining processes is challenging since collecting real-time high-frequency process data from data sources such as dynamometer sensors and processing collected data into data infrastructures to develop analytical models without latency and time-synchronization is required. Dynamometers are used to measure cutting torque and cutting forces occur between the workpiece and cutting tool during machining process. Collecting dynamometer data during machining is expensive in terms of sensor mounting, data acquisition and processing. To overcome this challenge, a method for cutting torque estimation that utilizes edge computing application to collect internal machine data is proposed in this thesis, to establish preliminaries for machining Digital Twin applications with edge computing. The cutting torque is estimated during drilling experiments and prediction errors are calculated for experiments with same workpiece material as 0.31% and 0.9%, and with different workpiece material as 1.02% and 1.25%. Edge device allows the collection of high-frequency machining process data coming from spindle and feed-drive motors by providing inbuilt network components that enables data acquisition to Cloud sources from machine. Edge device signals are also presented in servo motor current and position closed-loop control loop block-diagrams to demonstrate data flow stages from CNC machine tool's internal servo system to Edge device. The block-diagrams are validated with Edge signals collected during milling and drilling experiments.

Keywords: digital twin, edge computing, real-time data acquisition, internet of things, milling, drilling, servo motor monitoring, tool wear, hole quality, tool tip temperature, cutting torque estimation

ÖZETÇE

Yüksek Lisans Tez Başlığı

Cemile Beşirova

Makine Mühendisliği, Tezli Yüksek Lisans

16 Ocak 2024

CNC işleme süreçleri için Dijital İkiz uygulama geliştirmesi, dinamometre sensörleri gibi veri kaynaklarından gerçek zamanlı yüksek frekanslı süreç verilerinin toplanması ve toplanan verilerin gecikme ve zaman senkronizasyonu olmadan analitik modeller geliştirmek için veri altyapılarına işlenmesi gerektiğinden zorludur. Dinamometreler, işleme prosesi sırasında iş parçası ile kesici takım arasında oluşan kesme torkunu ve kesme kuvvetlerini ölçmek için kullanılır. İşleme sırasında dinamometre verilerinin toplanması, sensör montajı, veri toplama ve işleme açısından pahalıdır. Bu zorluğun üstesinden gelmek için, bu tezde, Uç Bilişim ile Dijital İkiz uygulamalarının işlenmesine yönelik ön hazırlıklar yapmak amacıyla, dahili makine verilerini toplamak için Uç Bilişim uygulamasını kullanan bir kesme torku tahmini yöntemi önerilmektedir. Delme deneyleri sırasında kesme torku tahmin edilmiş ve aynı iş parçası malzemesiyle yapılan deneylerde tahmin hataları %0.31 ve %0.9, farklı iş parçası malzemesiyle yapılan deneylerde ise %1.02 ve %1.25 olarak hesaplanmıştır. Uç bilişim cihazı, makineden Bulut kaynaklarına veri alımını sağlayan dahili ağ bileşenleri sağlayarak, iş mili ve besleme tahrikli motorlardan gelen yüksek frekanslı işleme süreci verilerinin toplanmasına olanak tanır. Edge cihazı sinyalleri ayrıca CNC makinesinin dahili servo sisteminden Uç Bilişim cihazına kadar veri akış aşamalarını göstermek için servo motor akımı ve konum kapalı döngü kontrol döngüsü blok şemalarında da sunulur. Blok diyagramlar, frezeleme ve delme deneyleri sırasında toplanan Uç Bilişim uygulaması sinyalleriyle doğrulanmıştır.

AKNOWLEDGEMENTS

I am thankful to my family for their constant support and their influence on my thinking, special thanks to Saida, Elmar and Metin Beşirov. Also, I would like to thank my beloved friends for encouraging me.

I would like to thank my colleagues from Koç University Manufacturing and Automation Laboratory Gamze Keçibaş, Reza Chehrezad and Waseem Akhtar, from Ford Otosan Uğur Üresin and Alper Şahin, from Siemens Mümin İrican, for their contribution to research.

I would like to thank Ford Otosan for supporting this research within AITOC (Artificial Intelligence supported Tool Chain in Manufacturing Engineering) and Siemens for supporting this research by Siemens Edge IoT Research Lab at Koç University.

Last but not least, I would like to thank my supervisor Prof. İsmail Lazoğlu for his guidance through my academic studies and my research.

TABLE OF CONTENTS

LIST OF TABLES

LIST OF FIGURES

ABBREVIATIONS

CNC	Computer Numerical Control
DT	Digital Twin
PLC	Programmable Logic Controller
HMI	Human Machine Interface
NCK	Numerical Control Kernel
NCU	Numerical Control Unit

Chapter 1:
INTRODUCTION

As industrial processes are getting evolved, an inclination arises towards merging physical and networked components and having an understanding upon processes from the data, in Industry 4.0 age. Industry 4.0 is explained as a dynamic system that employ control the integrated value chain of product lifecycle. Cyber-Physical Systems (CPP), Industrial Internet of Things (IIoT), Automation and Industrial Robots, Simulation and Modeling are enabler technology trends of Industry 4.0 vision [1,2]. Among them, Cyber-Physical Systems differentiate with having interactive physical components, contrary to conventional embedded systems with independent elements. With developments of CPSs specifically in manufacturing, Cyber-Physical Production Systems (CPPS) raised [3]. CPPSs are associated with Industry 4.0 since the term has initiated with concept of connecting physical factory systems in a cyber environment. CPPSs contains techniques such as smart designing which utilizes CAD and CAM tools, smart monitoring for conducting the maintenance of assets and smart control that utilizes industrial communication platforms to supervise machinery and equipment within factory, and smart machining that operates robots and sensors to manufacture parts. The elements of smart machining have surged in popularity in intelligent industries since these tools are providing precise and adaptable operations [4]. When it comes to the machining operations, CNC machine tool, which can perform dynamic movements across multiple axes and produce individual components, can be used for flexible manufacturing processes. To manage operations in manufacturing devices and systems, the “Machine Control” is denoted as fundamental concept as a part of deployment of smart machine models. An elemental concept of machine control is closed-loop systems, which in control theory, works with feedback of the measured output of the objective system that is controlled by a controller with logic [5].

One of the key concepts of Industry 4.0 is Digital Twins (DT), which became popular in recent years. Digital Twin is a virtual representation of a physical system with integrated multi-physics and probabilistic simulation, that utilizes optimum feasible models and physical measurement updates to imitate physical object to digital object with bidirectional data flow [6]. Likewise Cyber-Physical Systems (CPS), Digital

Twins are oriented towards realizing the fusion of cyber and physical components, which is a crucial aspect of smart manufacturing. However, functional implementations of these two concepts differentiates, since essential components of CPSs are sensors and actuators, whereas Digital Twins give priority to data and models [7]. The remarkable features of Digital Twin concept can be summarized in 1- Real-time mirroring of physical and digital systems, 2- Collaboration and integration in physical system; between historical and real-time data; between physical and digital systems, 3- Auto-development with ongoing advancement across physical and digital systems [8]. To perform complex tasks in real-time -especially in machining processes which requires high speed production- a high performance computational resource, data acquisition with minimum latency, a robust closed-loop control model is required for a Digital Twin. To create a feasible mechanism for precise quality monitoring, combining advanced simulations with online process data is becoming a target of new research.

In the field level of the Digital Twin, Edge Computing-based Digital Twins are initiated to be employed together with Cloud Platforms to handle process design optimization, quality control cycle and root cause analysis tasks next to physical system [9]. With Edge Computing concept, the processing platform is supplied in edge devices which locates near the data source. Thus, by utilizing edge and cloud computing in conjunction, a better performance can be achieved in real-time control scenarios and Cloud Computing burdens can be comforted [10]. The near-source and low latency features of Edge Computing makes it useful for Digital Twin applications especially for large and high-speed required physical systems in manufacturing such as machining.

In real-time control of manufacturing processes, especially in CNC machine tool systems, Digital Twins have potential by using process data to derive condition of cutting tools and workpiece during machining. Nonetheless, data-driven decision models for machining systems' Digital Twins are complicated to employ due to feasible real-world data for the twin being expensive [11]. For Digital Twin-embedded machine tools to perform tasks such as monitoring and autocorrect their actions, sensor signal-based Digital Twins must be maintained with CPSs. The prediction algorithms for tool condition monitoring such as tool flank wear prediction can also be implemented by using data collected from CNC machine tool [12]. However, the latency of the sensor signals should be considered to comprehend the dynamics when investigating the signals in both time and frequency scopes [13]. Considering fast and dynamic environment of the machining process, as well as the cost of reliable sensors that should be employed for condition monitoring, constructing a robust field for Digital Twin in machining becomes a challenging process.

The measurement methods to monitor machining process can be categorized as direct and indirect techniques. As an example of the direct measurement technique, sensors such as camera, laser beams and electrical resistors can be used for direct measurement of tool wear, which is crucial to estimate the remaining useful life of machine tools. On the other hand, with indirect measurements, the target value can be acquired by measuring supplementary assets [14]. Sensors that are used to measure acoustic emission, vibration and spindle torque can be utilized as indirect measurement technique for tool wear determination [15]. The rotary dynamometer sensors can used to acquire cutting force and torque data by locating on the cutting spindle. However, their usage is restricted to laboratory or research extend since this equipment is costly and special fixtures are required for the application [16]. Also, the cutting force and torque can be calculated by mathematical equations considering mechanics of metal cutting [14, 17].

In addition to the sensors, internal data can also be collected from CNC machine tool systems such as spindle drive power data, and machine control data as G codes to use in Digital Twin applications such as tool condition or tool breakage monitoring. One of the advantages of internal machine data over the sensor data is that external measurement systems are detached from CNC machine tool system, and it can be challenging to link these signals with respective task details [18]. In new generation multi-axes CNC machine tool systems, the internal data include signals of spindle and feed drive data, status and control signals, tool management and user program data [19]. To feed the data to Digital Twin models, the data source and information passing through the signal needs to be addressed. To fulfill this need, the signals can be represented in block-diagrams. From block diagram of the spindle motion control system, the transfer functions can be derived to determine parameters such as friction and disturbance torque [20]. Extracting data from the signals transferred between CNC machine tool system controller parts can allow monitoring cutting conditions. To collect high-frequency internal machine data from drives, Edge Computing solutions are integrated into machine tool to a greater extent. Thus, Machine Learning use-cases can be employed with this huge data collected with Edge Computing solutions [21].

The cutting torque during machining can be estimated by using internal drive current commands in CNC machine tool systems. Using electromechanical principles and cascade control structure of spindle drive, the block diagram and associated transfer function can be constructed to estimate cutting torque [22]. Cutting forces are transferred to feed drive motors through drive structure and servo system as disturbance torque. To evaluate the load spent during the cutting process from current commands, friction and internal loads that are utilized for the machine rigid body motion, needs to be partitioned [22, 23, 24]. The spindle-column system has elements with non-linear characteristics, and it consists of a column, a ball screw support bearing, two roller linear guides, spindle head, spindle system and tool holder. The equivalent dynamic model of this structure diagram constructs the system between servo drive and cutting tool [25]. Thus, the torque exerted by the spindle motor dissipates within those components until it reaches to the cutting tool and workpiece. These nonlinear features make it challenging construct a robust model for cutting torque with spindle current.

In this study, the data acquisition setup for CNC machine tool system, integrated with Industrial Edge and definitions of the collected signals are detailed in section 2; position control of feed drive system in terms of block diagram of signals are explained and validated in section 3; current and torque characteristics of spindle drive system are shown and linear spindle speed current region is defined in section 4; average cutting torque is estimated by estimating mechanical parameters of the spindle drive system and validated section 4; and finally conclusion and discussions is interpreted in section 5.

Chapter 2:
CNC MACHINE TOOL SYSTEM WITH INDUSTRIAL EDGE

2.1 Data Acquisition Setup

The CNC machine tool system comprises of NCK (Numerical Control Kernel), the PLC (Programmable Logic Controller) and HMI (Human Machine Interface) from a functional standpoint. Within them, the NC kernel is denoted as basis component of the system. The NC kernel manages the servo drive system that enables the machining of the workpiece by reading the part program and utilizing it to execute the main functions such as interpolation, position control and error handling. The PLC is initiating the control of the machine behavior except for the servo control, by continuously controlling the input and output signal processing, motor drive speeds, cutting tool, and workpiece adjustments. The NC kernel and PLC differentiates in machine control tasks since the NC kernel is dealing with the servo and drive control, whereas the PLC is responsible for the logic control. The final unit, HMI, provides an interface to integrate the NC and the user by showing the machine condition on display, providing tools for part program modification, and implementing the command for machine operations [26].

In this study, the 5-axis Spinner machining center implemented with SINUMERIK 840D sl CNC controller and Industrial Edge are used together as CNC machine tool system. The NC unit of the controller contains; NC kernel, PLC, drive, HMI, and communication processor with internal communication bus [27]. Industrial Edge platform can be used for collecting and processing high-frequency machine data in real-time applications along with machine tool controller together with built in MindSphere cloud connectivity [28]. Further in this paper, CNC machine tool system and Industrial Edge will be denoted as CNC and Edge for the simplification, respectively.

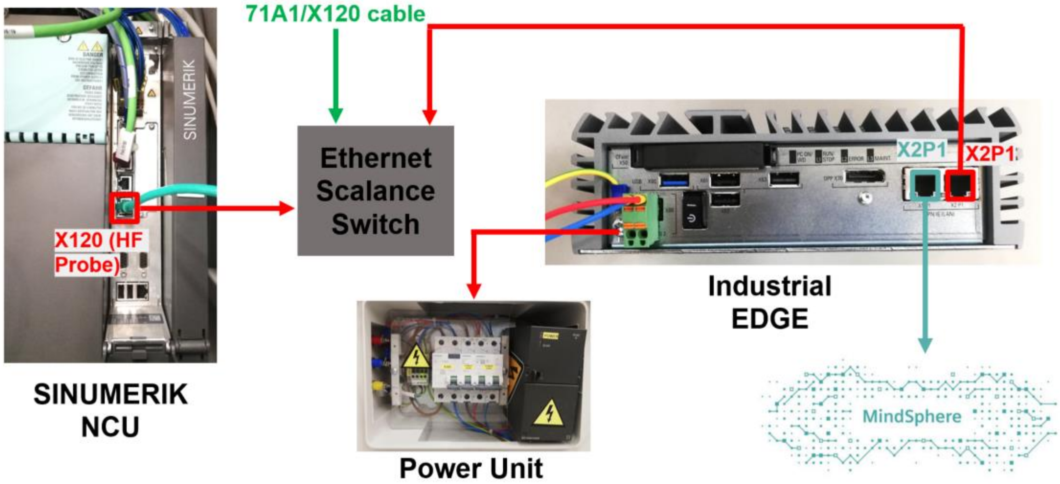

Figure 2.1: Connection scheme of CNC and Edge.

In Figure 2.1, the connection scheme of CNC and Edge are shown. Edge has two ethernet ports as for machine and external interface. The industrial ethernet port dedicated to machine interface of edge is connected to industrial ethernet port of the NC unit that is utilized for the connection to the system network through a network switch. Edge platform provides connectivity between automation and IT systems with benefits of Cloud. The Edge that is used in this study is an industrial PC, which has Linux operating system. Edge applications can run in the Edge environment that supplies tools for insulating, machine and factory network separation, packaging, provisioning, and updating applications [28]. In this study, two different industrial application run inside Edge are analyzed. The aim of the first application is to acquire high-frequency CNC data with 500 Hz sampling rate. Whereas the second application provides low-frequency drive signals of axis motors. In Figure 2.2, the basic structure of the first application that reads high-frequency drive signals is shown. The data comes from CNC controller flows through internal Databus. The application container reads high-frequency data and writes it to Samba Share, which is used to transfer files in Linux operating system [16].

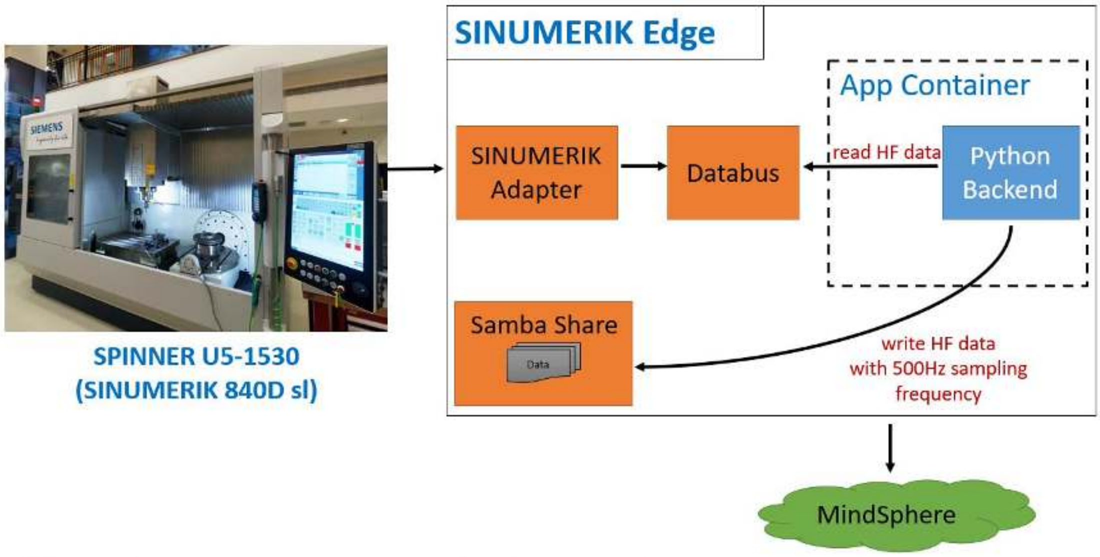

Figure 2.2: High-frequency data collection application runs inside Edge.

The second application that collects low-frequency drive data also writes the Payload to Samba Share. Definitions of high-frequency and low-frequency drive data that are collected from Edge applications are listed in Table 2.1 and Table 2.2, respectively.

2.2 Definitions of Datapoints collected from Edge Applications

The spindle and feed drive data can be used to gather knowledge about the condition of the machine tool system. The cutting force that is generated during machining operation between workpiece and the tool, also effects the spindle and feed drive data within position, speed, current, load and power related signals. When a cutting force is generated, the motors need to produce more mechanical power, thus, more electrical power and current to handle the machining operation. Also, due to forces, the servo motors positional and speed errors increase. Those parameters give insights about the machining process. Table 2.1 and Table 2.2 are showing the drive data be collected from Edge. The signals that are generated from drives are exchanged with NC kernel through special telegrams of internal bus [27].

Table 2.1: Definitions of high frequency datapoints collected from Edge [28, 29].

Datapoint	Description	Unit
Desired position	Desired position, position command after the fine interpolator	mm/deg
Controller input position	Position at the input of the position controller	mm/deg
Contour deviation	Contour deviation	mm/deg
Encoder position	Actual position of the active encoder	mm/deg
Position controller difference	Position controller input difference without DSC compensation	mm/deg
Velocity feedforward	Velocity feedforward to be added to the position controller output	mm/s or deg/s
Torque feedforward	Torque or force feedforward value that sent to drive from NC	Nm or N
Speed command	Speed command that sent to drive from NC	mm/s or deg/s
Actual current	Actual drive current	A
Torque setpoint	Torque setpoint sent to current setpoint filter	Nm or N
Load	Drive load as a percentage	%
Power	Actual power of the drive	W

Table 2.2: Definitions of drive datapoints collected from Edge [28, 29].

Datapoint	Description	Unit
Actual speed smoothed	Smoothed actual value of motor speed	rpm, mm/min
Smoothed absolute current	Smoothed absolute actual current value	A rms
Temperature	Actual temperature in motor	°C
Actual quadrature-axis current	Actual torque-generating current of the drive	A rms
Torque utilization	Torque utilization as a percentage	%

Edge provides position, speed, current, torque, load, and power dependent data of transitional and rotational axis motors of the CNC. The axis motors of the CNC are permanent magnet synchronous motors. CNC internal cascade servo closed-loop control structure that contains position control loop in NC kernel, speed, and current control loop in drive, together with speed and torque feedforward control as shown in Figure 2. The position controller output is processed to motor drive which moves the servo motor by controlling speed and torque values. At the end the servo motor generates movement in machining process [26].

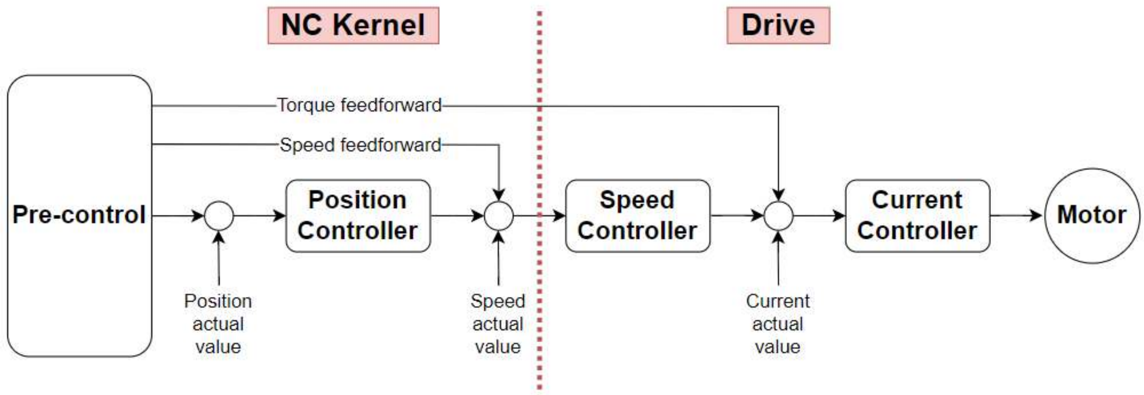

Figure 2.3: Torque feedforward control block diagram in NC kernel and drive [19].

The main purpose of the feedforward control is to reduce axial following error, which indicates the difference between desired and actual position of the machine axis. The following error varies in accordance with the square of the feedrate, and the main source of this error is servo delay. The position controller gain can be incremented to lessen the following error, nonetheless, this can create vibration and produce unstable operation. In cascade control loops, the outer loop response is slower than the inner loop. According to this, the feedforward controller outputs are processed to inner loop precisely. Thus, the outer loop response is becoming better with the feedforward structure [26]. By adding additional velocity setpoint, which is being equal to given spindle speed or feedrate by G-code, following error can almost be eliminated. On the other hand, additional torque feedforward value is determined using moment of inertia [19].

Chapter 3:
CASCADE CONTROL SCHEME WITH INDUSTRIAL EDGE SIGNALS

3.1 Position Control of Feed-drive System

The signals that are processed in NC kernel consist of position related signals as detailed in the previous chapter. To analyze position related signals, the transitional axis drive signal on the feed direction during cutting operation will be used to observe following error during curvatures clearly.

3.1.1 Closed-loop Block Diagram for Position Control

As detailed in this section, according to the signal definitions in datasheets and the collected experimental data from Edge, the associative Edge signals in this position control block diagram are determined [19, 28]. The closed loop position control block diagram of an axis/spindle in NC kernel is shown in Figure 3.1. Some datapoints that can be captured with Edge are represented in associated signals in the overview diagram of axis spindle information. Upon examining Figure 3.1, the diagram starts with fine interpolator, which reads the interpreted data of the part program and computes the position and velocity for each unit time of axes [26]. With fine interpolator, by decreasing ladder effect in speed setpoint, thus the contour precision can be enhanced additionally. The datapoints generated after fine interpolator is desired position. When program is executed in the controller, position, and velocity setpoints are sent from path control interpolator to FIPO (fine interpolator). In FIPO, by decreasing ladder effect in speed setpoint, thus the contour precision can be enhanced additionally [19].

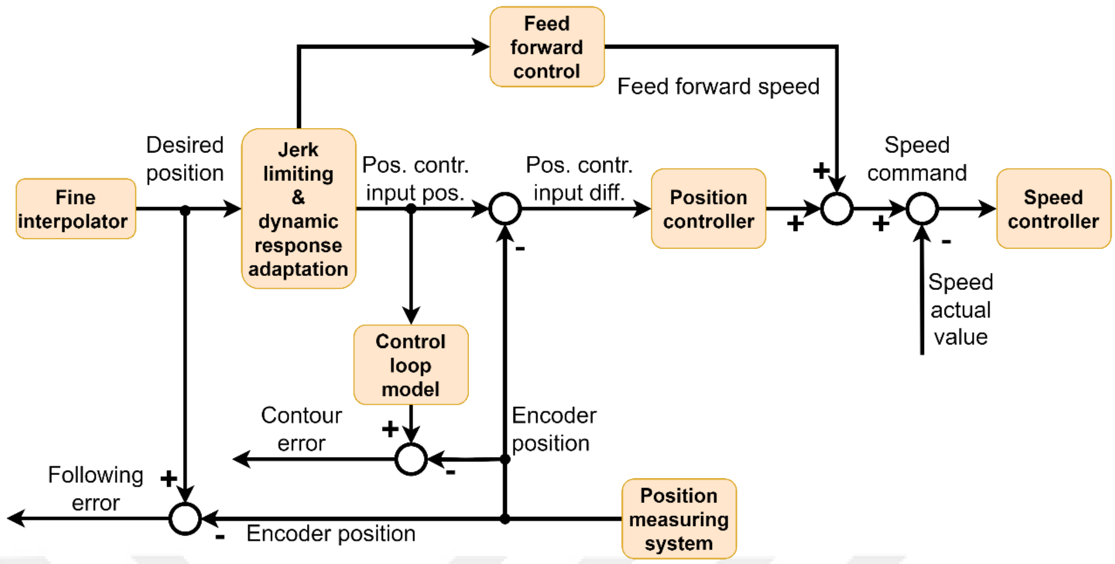

Figure 3.1: Position control loop block diagram in NC kernel [19].

In jerk filter block, position setpoint characteristic of a machine axis is smoothed to improve surface quality of the workpiece by reducing mechanical vibrations generated in the machine. This filter has lowpass characteristics and rounds a contour at the center of curvature. In dynamic response adaptation block, position controller servo gain factors of the axes, which interpolate with one another, can be set to the same following error by reducing servo gain factors to the axis of minimum dynamic performance. With this functionality, optimum contour accuracy can be attained. Thus, the contour error that arises from position control signal deformations can be decreased. The phase filter block applies a pure phase shifter for setpoint phase response. Amplitude response and phase response can be adapted independently of one another together with jerk and phase filter. The difference between the desired position and the actual position of the machine axis is defined as following error, also known as the system deviation, when traversing a machining axis. This following error can lead to undesired velocity-dependent contour violations, especially at acceleration in contour curvatures such as circles and corners. The following error increases initially at acceleration phase, after a time the following error becomes constant depending on position control parameters [19, 30].

3.1.2 Validations of Position Control with Edge Signals

To validate the effects of the functions in position control loop, a milling experiment has been conducted with square and circle shaped tool path. The cutting tool has followed a square and circle tool path on the Al7050-T7451 workpiece with 0.5 mm axial depth of cut. In the experiment, aluminum is cut with 16 mm diameter 2 flute carbide milling tool. Feed per tooth during experiment was 0.167 mm/tooth.

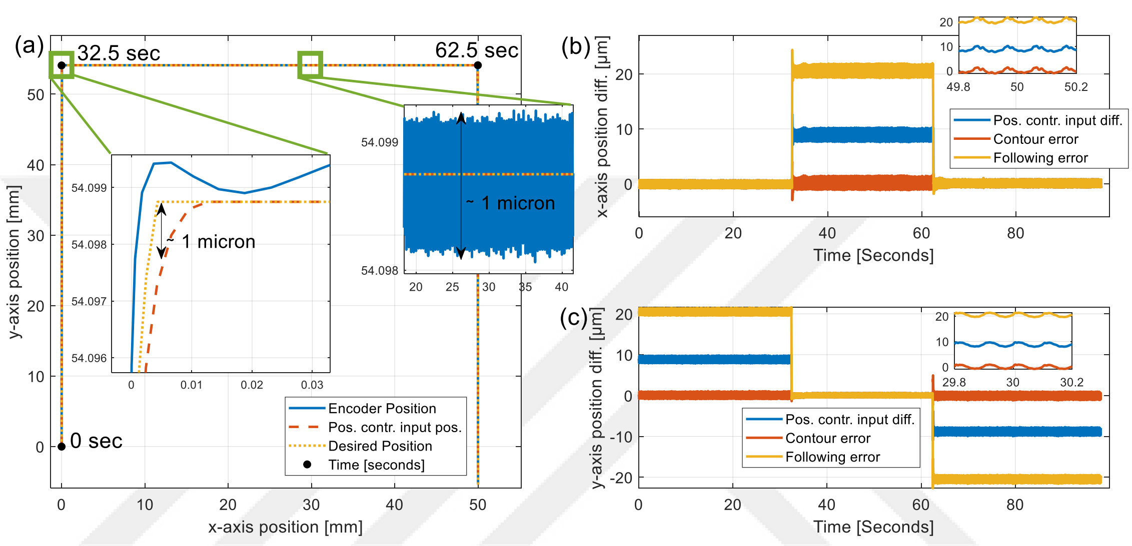

Figure 3.2: Milling operation on squared-shaped tool path: (a) tool path with position related signals (b) x-axis positional error related signals (c) y-axis positional error related signals.

In Figure 3.2a, encoder position, controller input position and desired position datapoints on x and y axes are shown on the square shaped tool path. A jerk filter, dynamic response function and phase filter functions applied after desired position signal to construct controller position, as it previously has been shown in Figure 3.1. The experimental data validates that filtrations after desired position allow tool path to be smoother in position controller input position. Also, when the tool path reaches to the corner shape, the difference between actual position and the commanded positions are increasing.

Position controller input difference is the positional reference given in the input of the position controller. It has validated from experimental data that this signal equals to the difference of controller input position which is desired smoothed trajectory and encoder position. In Figure 3.2b and Figure 3.2c, controller difference and contour error can be seen for x and y axes, to observe the effect of the control loop model function that is applied to controller difference to construct contour error. While following error and position controller input difference signals are showing trend of corner shaped tool path, contour error is deviating around 0.

To detect the difference between positional difference related signals, the circle shaped tool path is also observed. In Figure 3.3a, the encoder position, controller input position and desired position datapoints on x and y axes are shown on the circle shaped tool path. In Figure 3.3b and 3.3c, positional controller input difference and following error signals shows trend of circular tool path, while contour error is deviating around 0, as shown previously in different tool path in Figure 3.2. The reason of this is that following error and positional controller input difference shows the difference between actual tool position and desired tool position. On the other hand, contour error shows the deviation of cutting tool from desired cutting path.

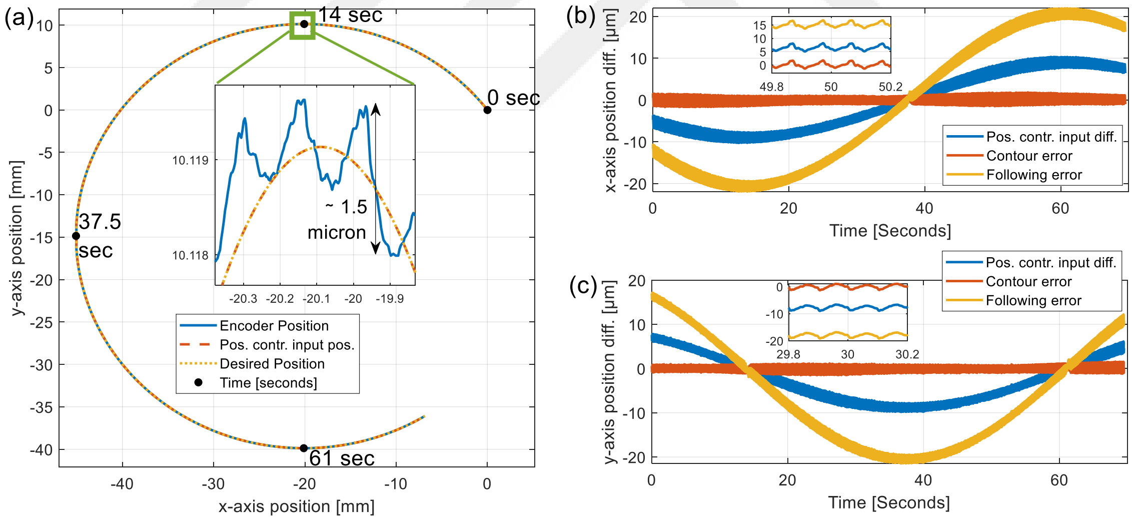

Figure 3.3: Milling operation on circle-shaped tool path: (a) tool path with position related signals (b) x-axis positional error related signals (c) y-axis positional error related signals.

3.2 *Current Control of Feed-drive System*

Current control scheme is analyzed for the rotational axis spindle to calculate cutting torque which has a significant correlation with spindle current. Through the spindle and feed drive motor design parts and servo drive, the forces that are produced at the cutting tool conveyed to the spindle and feed drive motors as disruptive torque. This disruptive torque in motor is arising from dynamic loads generated by acceleration and cutting forces. On the other hand, the static loads comprise of the friction of elements such as ball screw, bearings through kinematic chain. In Eq. 1., the total mechanical torque of servo motor that is tiring out of these static and dynamic loads can be given [22]. The total mechanical torque (τ_m) of spindle motor that composed (B) viscous friction coefficient, (Ω) spindle angular velocity, inertia (J), Coulomb friction (τ_f) and cutting torque (τ_c). (τ_m) is also directly linked to motor current (I) and torque constant (K_T).

$$\tau_m = B\,\Omega + J\frac{d\Omega}{dt} + \tau_f + \tau_c = K_T\ I \tag{3.1}$$

3.2.1 *Closed-loop Block Diagram for Current Control*

The basic closed-loop current control block diagram of an axis/spindle in drive together with power and DC voltage signals is shown in Figure 3.4. This simplified block diagram is constructed by summarizing several servo and vector control function diagrams from datasheets of CNC and drives [30, 32, 34]. The spindle motor in the machine is PMSM (Permanent Magnet Synchronous Motor).

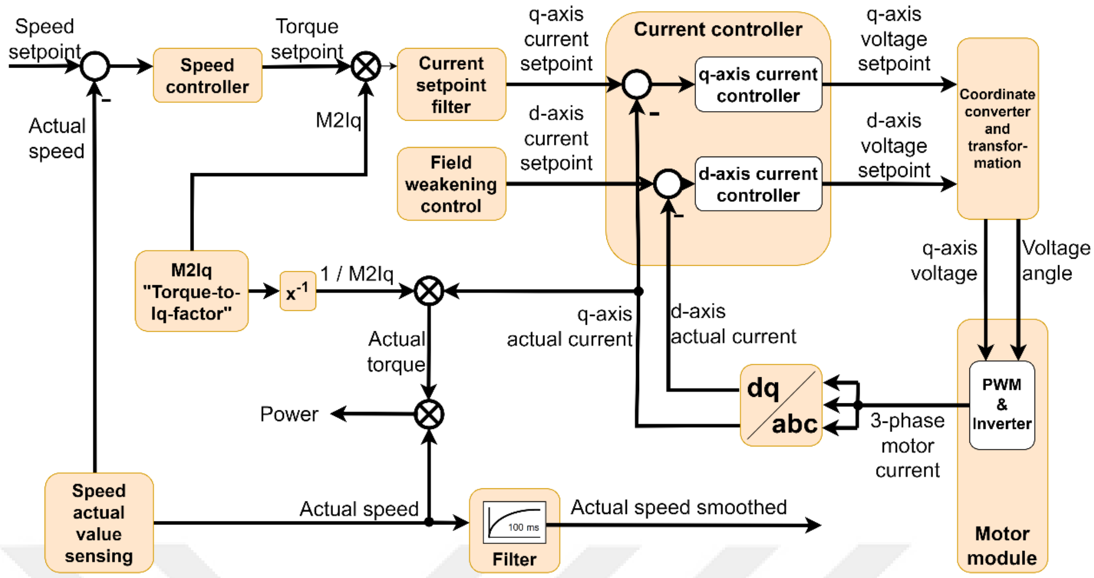

Figure 3.4: Current control loop of spindle drive [19, 29]

As shown in Figure 3.4, in control loop, an initial torque setpoint is generated at the output of the speed controller. Afterwards, this initial torque setpoint value is being processed into control type changeover and limiting operations with torque pre-control values. Following that, the torque setpoint value is produced, also the quadrature-axis current setpoint is calculated by multiplying torque setpoint and torque factor.

In general, the PMSM has a closed-loop control system that is placed on vector control method. In vector control, three phase stator currents are decoupled into quadrature-axis and direct-axis currents, which can also be called as torque-generating and field-generating currents. Those quadrature-axis and direct-axis currents are generating torque and flux, respectively. As depicted in Figure 3.4, the direct-axis current setpoint is generated from field weakening control function. In field weakening control strategy, stator current is limited by voltage limit circle and current limit circle [31]. To reduce rotor flux, negative direct-axis current is applied in the stator in field weakening control. Thus, quadrature-axis stator current is decreasing as well as the electromagnetic torque [42].

With coordinate and converter transformation block on the same diagram, quadrature-axis, and direct-axis voltage setpoints that have been generated at the output of the current controllers are transformed into actual output voltage of the power unit and voltage angle, afterwards those values are processed in motor module. 3-phase current that actual values are generated from motor module is subjected to Park transform which is converting 3-phase currents to actual values of direct-axis and quadrature-axis currents. Actual quadrature-axis current is collected as Edge drive datapoints.

The absolute current is calculated with actual quadrature-axis current and actual direct-axis current. The smoothed actual current is collected as Edge drive datapoints. The actual drive torque is calculated by dividing actual quadrature-axis current with torque factor, following that, the drive power is evaluated by multiplying actual drive torque and drive actual speed. The actual speed smoothed with 100 ms smoothing time constant is captured as Edge drive datapoints. It should also be emphasized that there can be a significant amount of difference between drive datapoints which shown in Figure 3.4 and high-frequency Edge datapoints due to the data and function interface, signal exchange rules and configured time span for the data exchange between NC, PLC and drives in CNC [19].

3.2.2 Validations of Current Control with Edge Signals

Drilling operations are conducted and spindle motor data from Edge device collected to understand the relations of datapoints shown in current control loop, in Figure 3.4. In addition to Edge datapoints, cutting torque signals from Kistler rotary type dynamometer is collected. The experimental setup is shown in Figure 3.5. The cutting tool is carbide tool with TiAlN coating and 8.5 mm diameter. Two different workpiece materials were used as type A graphite flake cast iron brake disc and AISI 1045 carbon steel plate. CutPro software and NI data acquisition device is used to process the analog signals coming from rotary type dynamometer. The cutting force and cutting torque analog signals from rotary dynamometer are sent to signal conditioner. Afterwards, the amplified signals are sent to NI acquisition device to acquire digital output. Finally, the cutting force and torque data can be seen and analyzed in CutPro Software.

The datapoints collected from Edge and dynamometer is put together in Matlab with cross-correlation algorithm. Since two different data sources are used in data collection, data coming from two sources should be merged in common time axis. With cross-correlation algorithm, the time-series data is merged.

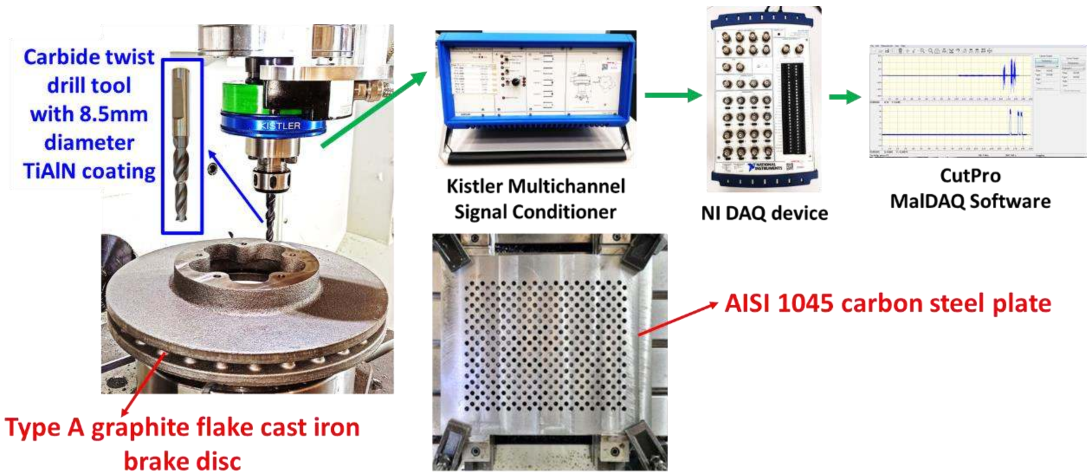

Figure 3.5: Data acquisition setup of rotary type dynamometer during drilling cast iron brake disc and steel plate.

In Figure 3.6., the datapoints collected from Edge and dynamometer during drilling cast iron brake disc with 2400 rpm spindle speed and 0.3 mm/rev feedrate is shown together. The sample rate is 2 milliseconds. When low-pass filter is applied, the similar trend between signals is visible.

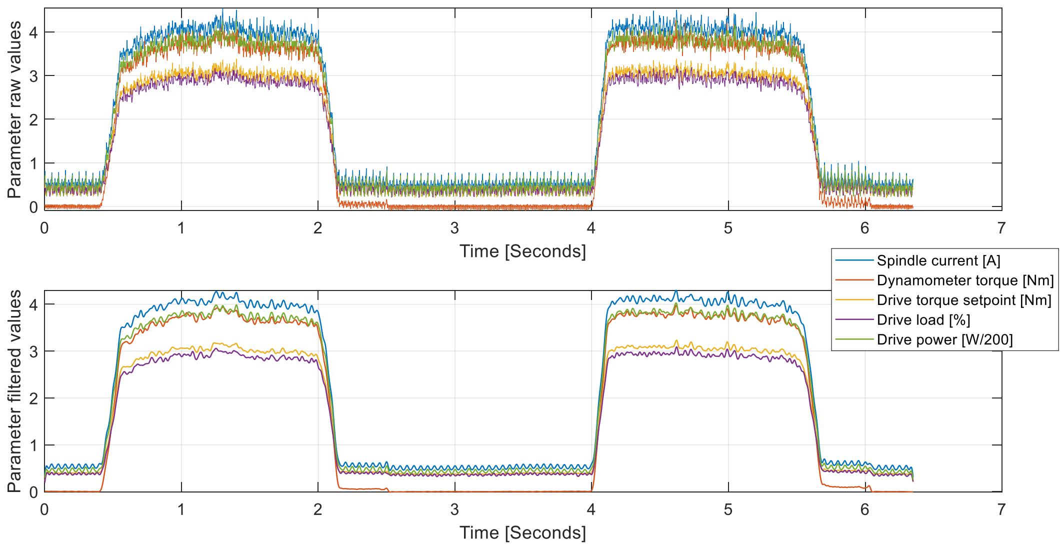

Figure 3.6: Drive datapoints shown in closed-loop current control scheme collected from Edge and dynamometer during drilling cast iron brake disc with 2400 rpm an 0.3 mm/rev feedrate a) raw values b) low-pass filtered values with 10 Hz band pass frequency.

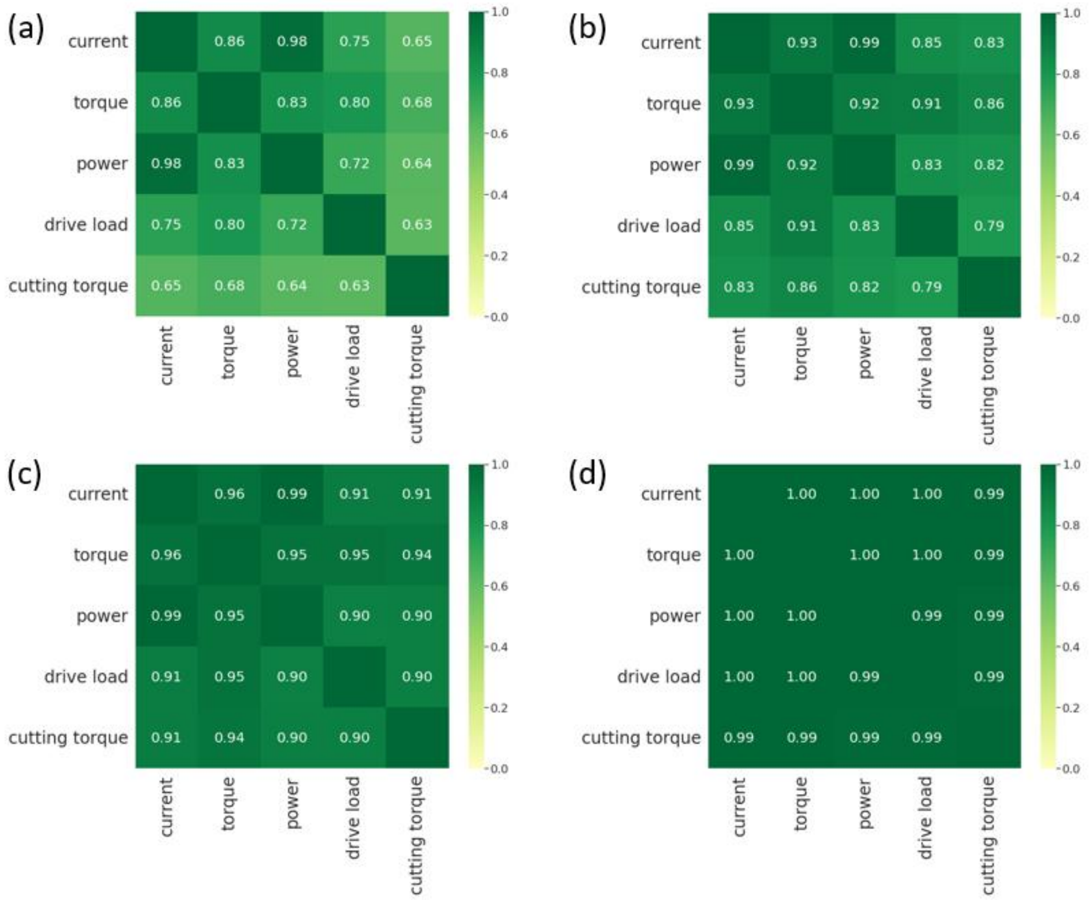

Figure 3.7: Heatmap of correlation matrix of spindle drive datapoints collected from Edge and cutting torque collected from dynamometer during cast iron drilling experiment with 2400 rpm spindle speed and 0.3 mm/rev feedrate a) raw data b) low pass filtered data with 100 Hz cut off frequency c) low pass filtered data with 50 Hz cut off frequency d) low pass filtered data with 10 Hz cut off frequency.

To comprehend the relations of different parameters, heat map of correlation matrix is shown in Figure 3.7. When low-pass filter is applied to Edge and dynamometer signals collected during drilling operation, the measurement and sensor noises are eliminated. Thus, the correlation between the parameters is increasing. It can be seen from Figure 3.7 that while correlation between parameters is low when raw drilling cutting region data is used. The correlation increases when cut off frequency of low pass filter decreases, as seen in Figure 3.7b, 100 Hz cut off frequency, 3.7c 50 Hz cut off frequency and 3.7d 10 Hz cut off frequency.

It can be seen from Figure 3.6 that, during air-cut, when the zero cutting torque is applied in the process, load, power, current and torque setpoint parameters collected from Edge are not equal to zero since the spindle motor is turning with constant cutting speed. The cutting torque and current is proportional to spindle speed, as shown in Eq. 3.1. To understand the relation between cutting speed and air-cut experiments collected with 126 different spindle speed experimentally, spindle drive run at 126 different speeds until 18000 rpm, since the maximum speed of the motor is denoted as 20000 rpm in its catalog. The mean, minimum and maximum values of the Edge datapoints during constant spindle speed with zero cutting torque is analyzed. In Figure 3.8, the mean, minimum and maximum values Edge datapoints collected during air-cut experiments is shown.

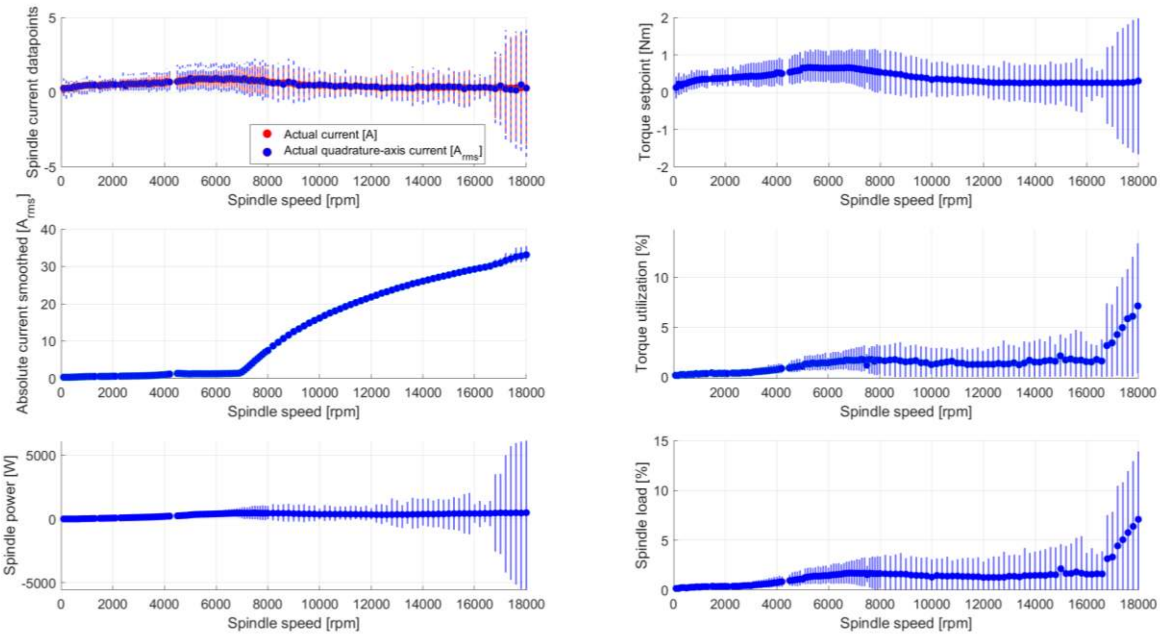

Figure 3.8: Mean, minimum and maximum values of datapoints collected from Edge during air-cut with different spindle speeds a) spindle current datapoints b) torque setpoint c) absolute current smoothed d) torque utilization e) spindle power f) spindle load.

It can be seen from Figure 3.8a that after 16800 rpm, the ripple increases; also, the average current values start to decrease after 7000 rpm, which is denoted as the speed at which field weakening starts, in the spindle drive characteristics. In Figure 3.8b, the spindle drive torque has similar characteristics with spindle drive current shown in Figure 3.8a. In Figure 3.8c, the actual absolute current starts to increase dramatically after 7000 rpm, since the field weakening starts at that speed, the field generating current starts to affect the absolute current. In Figure 3.8d and Figure 3.8f, the high-frequency load and low-frequency, drive torque or force utilization, parameters have similar characteristics. In Figure 3.8e, the spindle power has low fluctuation at low speeds, however after around 7000 rpm, the fluctuation can be visible from minimum and maximum values. To understand the relations in detail, a heatmap with mean values of the datapoints collected with different speeds is plotted in Figure 3.9.

From Eq. 3.1, it can be conducted that when zero cutting torque is applied to the process and if the friction parameter is assumed to be constant value, the spindle motor current should be proportional to the spindle motor speed. However, from Figure 3.8, the relation is not in every speeds. To validate the equation and estimate the cutting torque from spindle current by calculating the unknown parameters given in Eq. 3.1, experimentally, linear speed-current region will be found, and unknown parameters will be calculated with experimental data in next chapter.

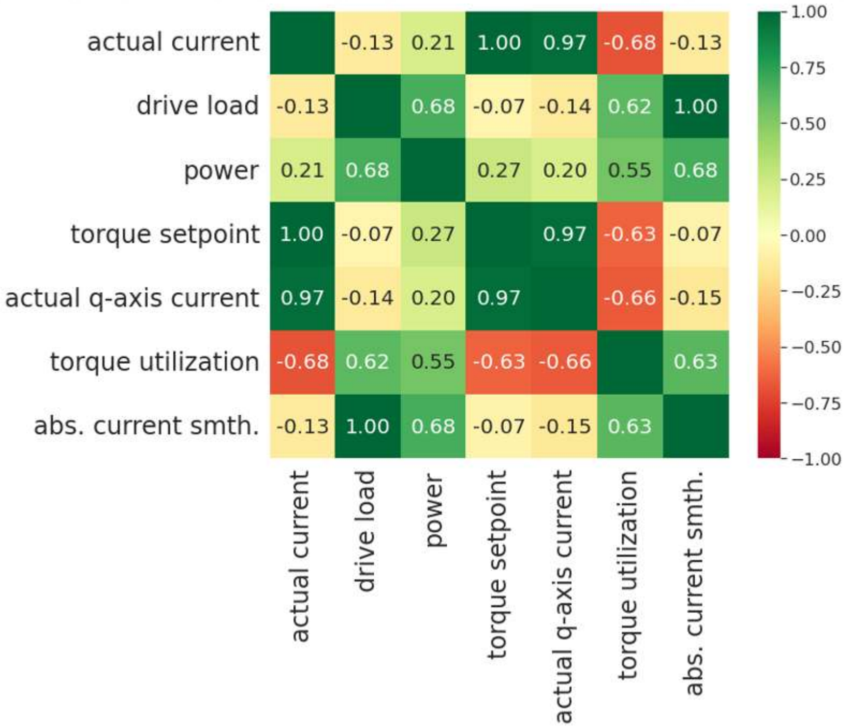

Figure 3.9: Heatmap of correlation matrix of mean values of datapoints coming from spindle drive collected from Edge during air-cut with 126 different spindle speed.

Chapter 4:
CUTTING TORQUE ESTIMATION WITH SPINDLE CURRENT

4.1 Finding Linear Speed – Current Region of Spindle Motor

In spindle drive system, there is field-weakening functionality available. Field-weakening or flux-weakening is executed to increase the efficiency of PMSM by enabling it to perform highest power by optimally adjusting the direct current of the motor [33]. In permanent magnet motors, the magnetic flux cannot be controlled straightforward. Although, with addition of demagnetizing current to the d-axis current, the air-gap flux can be reduced [34, 35]. The speed in which field-weakening starts is denoted as 7000 rpm in spindle motor datasheet. As shown previously in Figure 3.8, the datapoints given in current control scheme are affected by field-weakening after 7000 rpm.

Current limiting is another functionality that is present in spindle motor characteristics. To find the speed where the current limitation starts, the speed of the drive is increased during air-cut until the speed where the field weakening start, which is 7000 rpm according to drive parameter definitions, and q-axis current is recorded. In Figure 4.1, after 5000 rpm, q-axis current is not increasing proportional to the spindle speed. Thus, the beginning of the field weakening region can be found experimentally as 5000 rpm.

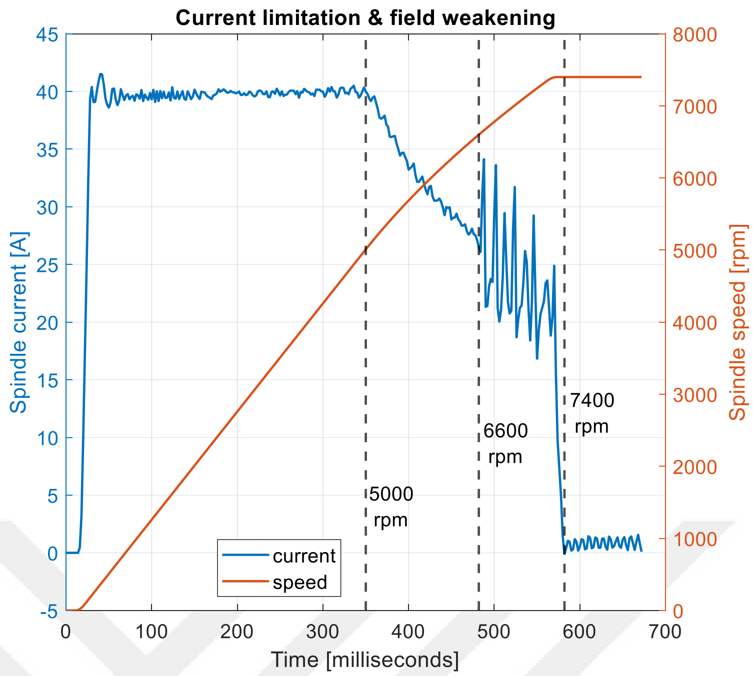

Figure 4.1: Current limitation and field weakening characteristics of spindle drive.

According to data shown in Figure 4.2, the upper limit of the linear speed-current region can be determined as 5000 rpm, where the current limitation starts, experimentally. The mean values of spindle current are also not demonstrating linear behavior at low frequencies of motor speed. To find the lower limit of the linear speed-current region, the datapoints are investigated in the frequency domain according to synchronous speed formula given in Eq. 4.1. In the formula, N stands for synchronous speed in rpm and p is the number of pole pairs. Therefore, when the speed and pole number is known, the frequency generated from stator can be found.

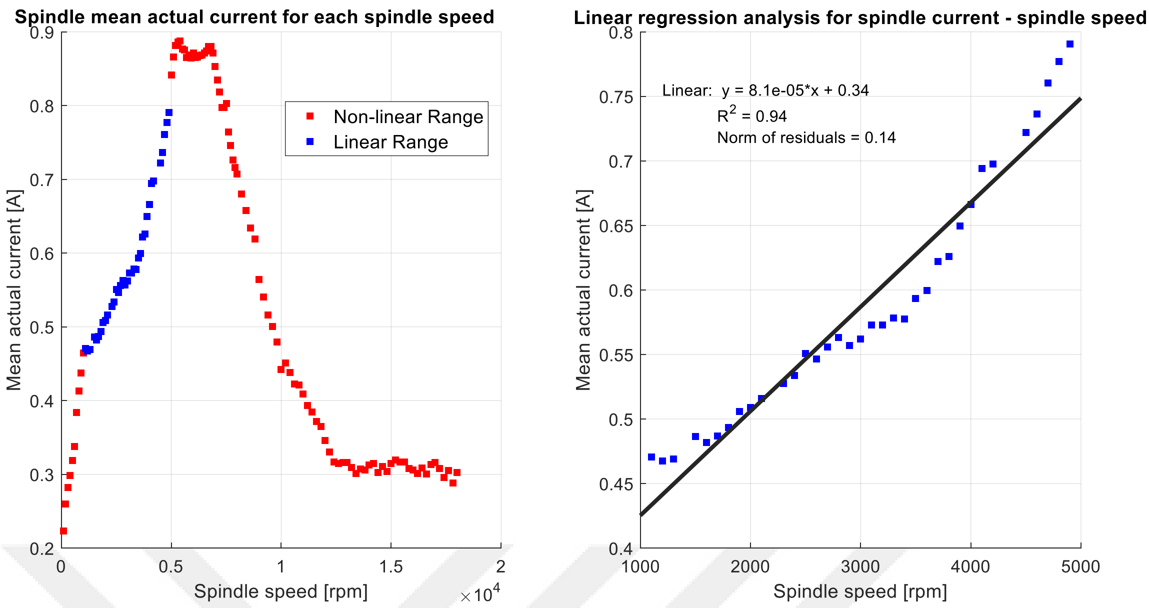

Figure 4.2: Linear regression analysis with actual spindle drive current values at different spindle speeds during air-cut.

$$f = \frac{N\,p}{120} \tag{4.1}$$

In Figure 4.3a, the stator frequency component of spindle current signal at 3200 rpm calculated and filtered. In Figure 4.3b, periodic signal coming from stator frequency component is subtracted from the original spindle current signal and displayed as filtered signal. In Figure 4.3b, the stator frequency is increasing amplitude of current signal by not affecting the average current. When the current datapoints at different speeds investigated in frequency domain, the datapoints with speeds lower than 1100 rpm is not displaying stator frequency as dominant frequency. Because of that is the lower limit of the linear speed-current region is determined as 1100 rpm, experimentally.

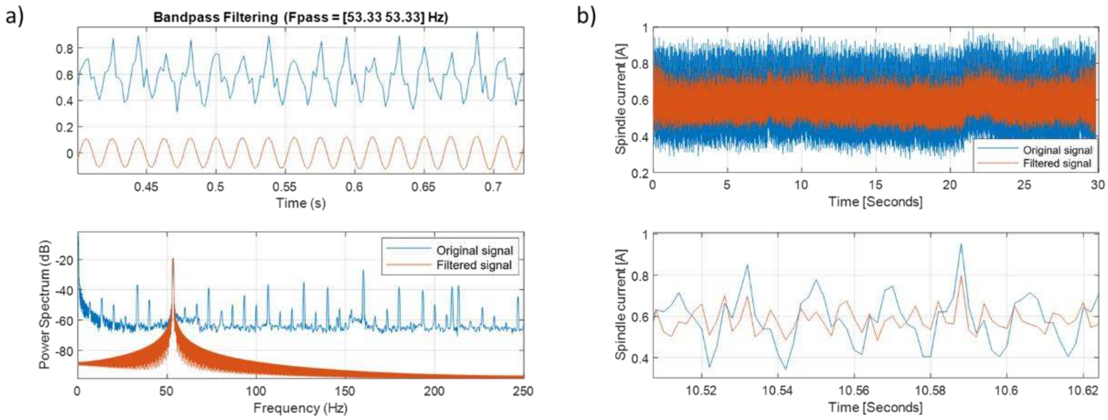

Figure 4.3: a) Bandpass filtering stator frequency from spindle current signal at 3200 rpm, b) Original spindle current signal together with the current signal in which the signal component coming from stator frequency is eliminated.

4.2 Motor Temperature Analysis

In addition to speed, the drive current can also be affected by some measurable parameters such as temperature, flux, motor resistance and inductance, also some unmeasurable environmental conditions.

To observe the effect of the temperature on the spindle drive current, the spindle has turned in 5000 rpm and 7000 rpm separately, more than 20 minutes and the Edge signals are recorded. In this period, the motor temperature has increased gradually. It can be seen in Fig. 11 that when the temperature is increasing the spindle drive current is decreasing.

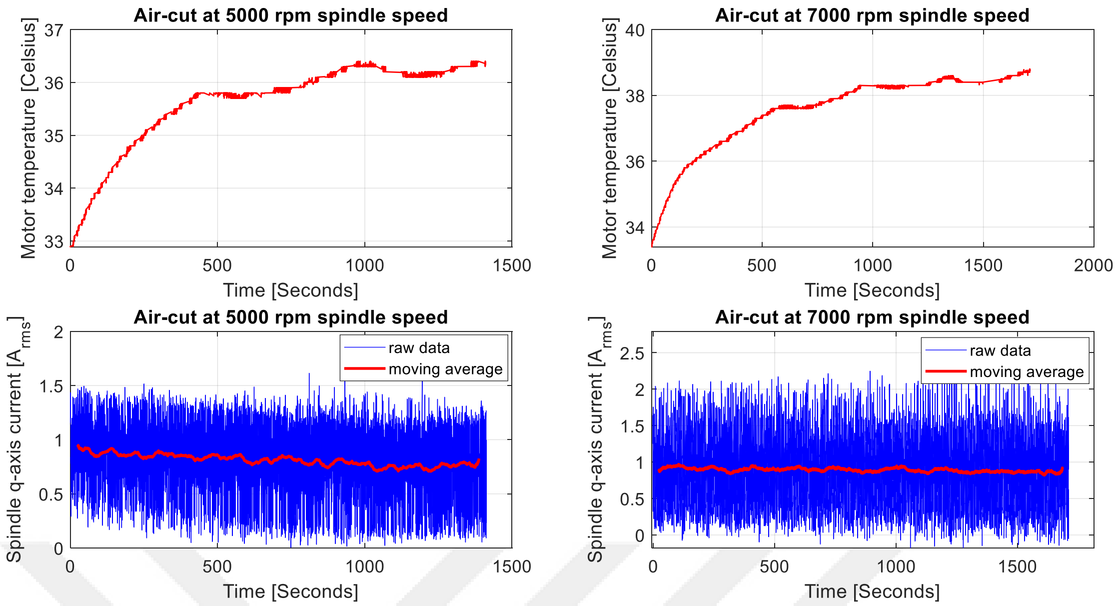

Figure 4.4: Spindle motor temperature and spindle actual current characteristics.

4.3 *Calculating Friction Coefficients for Cutting Torque Estimation*

In the previous section, the upper and lower limit of linear speed-current region is found as speeds at which current limitation starts in 5000 rpm and stator frequency starts to be dominant from 1100 rpm, respectively. Now, the unknown parameters in Eq 3.1 can be found experimentally by using the current datapoints collected from Edge. To find the B/K_T and τ_f/K_T parameter, a linear curve fitting is applied to the average q-axis current values between 1100 and 5000 rpm spindle speed as shown in Figure 4.2. The linear equation is shown Eq 4.1. The R^2 and norm of residuals values of linear equation are 0.94 and 0.14, respectively. According to Eq 4.1, B/K_T and τ_f/K_T are estimated as 8.1 10^{-5} $[Nm/rpm]$ and 0.34 $[Nm]$, respectively.

$$I\ [A] = 8.1\ x\ 10^{-5}\ \Omega\ [rpm] + 0.34 \tag{4.2}$$

According to mechanical torque equation given in Eq. 3.1, when there is no acceleration, the cutting torque constant can be calculated with Eq. 4.2. Since the cutting torque is measured with rotary type dynamometer and all the other parameters are known as well, the cutting torque constant by taking the cutting torque data collected during steel plate drilling experiment with 2400 rpm spindle speed and 0.16 mm/rev feedrate as ground-truth, experimentally. After calculating torque constant with experimental data, the estimated torque constant will be validated with other drilling experiments with different workpiece material, spindle speed, feedrate values.

$$K_T = \frac{\tau_c}{I - \frac{B\,\Omega}{K_T} - \frac{\tau_f}{K_T}} \tag{4.2}$$

In the Figure 4.5, cutting torque measurement with dynamometer and actual current data collected from Edge are shown during a drilling experiment. The mean current and torque values with datapoints collected during first 0.6 seconds of the cutting regions, in order not to be affected by environmental conditions such as increasing tool tip temperature due to friction.

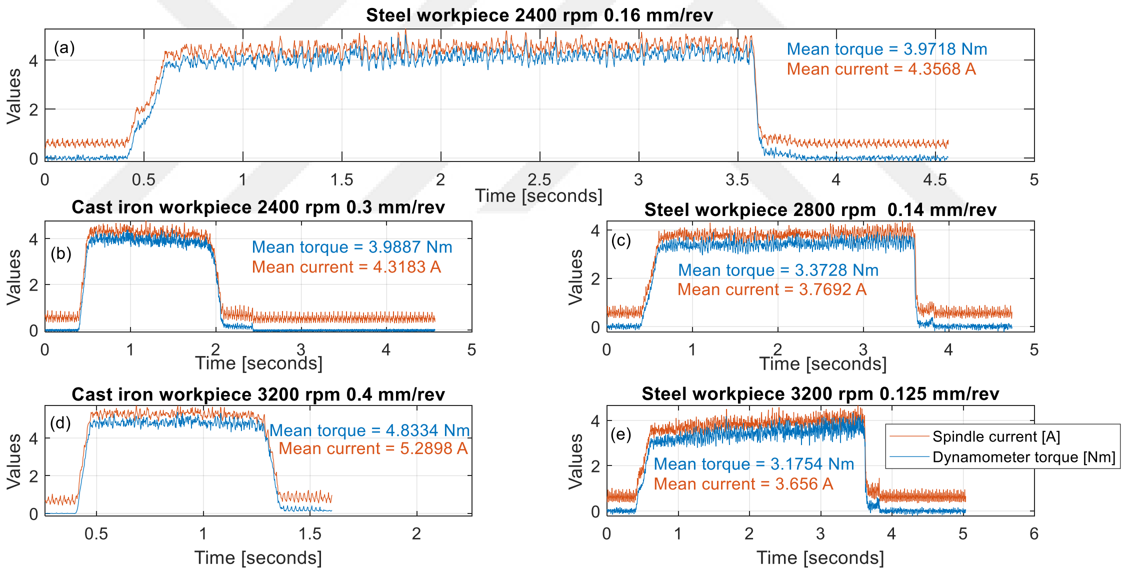

Figure 4.5: Dynamometer torque and Edge spindle current data collected from drilling experiments (a) steel workpiece 2400 rpm 0.16 mm/rev (b) cast iron workpiece 2400 rpm 0.3 mm/rev (c) steel workpiece 2800 rpm 0.14 mm/rev (d) cast iron workpiece 3200 rpm 0.4 mm/rev (f) steel workpiece 3200 rpm 0.125 mm/rev.

To find cutting torque constant, mean current and mean torque at the cutting region are calculated as 4.36 A and 3.97 Nm, respectively, during drilling steel workpiece at 2400 rpm and 0.16 mm/rev feedrate. Thus, according to Eq. 4.1 and Eq. 4.2, cutting torque constant is estimated as 1.28 Nm/A as shown in Eq. 4.3.

$$K_T = \frac{3.97}{4.36 - (8.1\ x\ 10^{-5}\ x\ \ 2400) - 0.34} = 1.04\ Nm/A \tag{4.3}$$

After estimating torque constant as 1.04 Nm/A, viscous friction coefficient (B) and Coulomb friction (τ_f) are estimated as $8.42 * 10^{-5}\ Nm/rpm$ and $0.35\ Nm$, respectively. Finally, the equation for estimating cutting torque at constant cutting speed with spindle current and mechanical parameters are found experimentally as given in Eq 4.4.

$$8.42\ 10^{-5}\ \Omega\ [\text{rpm}] + 0.35 + \tau_c = 1.04\ I[A] \tag{4.3}$$

4.4 *Validations with Cast Iron and Steel Drilling Experiments*

This predicted cutting torque constant parameter is validated with 4 different drilling experiments conducted with cast iron brake disc and steel plate with different spindle speed and feedrate values. The experiments for validation with measured and estimated values are shown in Table 4.1.

Table 4.1: Validations of cutting torque estimation with drilling experiments.

Workpiece	Spindle speed and feedrate	Measured mean spindle current	Measured mean cutting torque	Predicted mean cutting torque	Predicti on error
Cast iron	2400 rpm 0.3 mm/rev	4.32 A	3.99 Nm	3.94 Nm	1.25 %
Cast iron	3200 rpm 0.4 mm/rev	5.29 A	4.83 Nm	4.88 Nm	1.02 %
Steel	2800 rpm 0.14 mm/rev	3.77 A	3.37 Nm	3.34 Nm	0.9 %
Steel	3200 rpm 0.125 mm/rev	3.66 A	3.18 Nm	3.19 Nm	0.31 %

The cutting torque value is predicted according to experimental data collected during steel workpiece drilling experiment at 2400 rpm spindle speed and 0.16 mm/rev feedrate. According to that, it can be seen from Table 4.1 that the prediction error is more less when the mechanical friction parameters and torque constant validated with the same workpiece. However, the spindle speed is not affecting much to the prediction error. According to cutting torque and spindle relations given in Eq. 3.1, it can be concluded from the results shown in Table 4.1. that estimated parameters may vary according to the workpiece material used during the experiments.

Chapter 5:
DIFFERENT DIGITAL TWIN USE-CASES WITH EDGE COMPUTING

5.1 Tool Wear Detection

As tool wear in cutting tool increases, the cutting torque generated during machining operation increases, so that the spindle current value. To detect tool wear with spindle current data collected from Edge, a series of drilling experiments conducted with TiAlN carbide drill and AISI 1045 carbon steel workpiece. The drilling experiments conducted until the tool reaches around 277-micron flank wear. Total number of drilled holes is 2676 and each hole is 20 mm. The spindle speed during experiments is 2400 rpm, and the feedrate is 400 mm/min. The cutting torque data from dynamometer and high-frequency Edge datapoints are collected during experiments. The collected Edge data can be used with tool wear measurements taken by microscope to construct a supervised deep learning model to estimate tool wear. However, in production environment, measuring tool wear is not possible. To use the AI model for tool wear estimation, the model should be calibrated accordingly with historical machine data. The experimental setup can be seen in Figure 5.1.

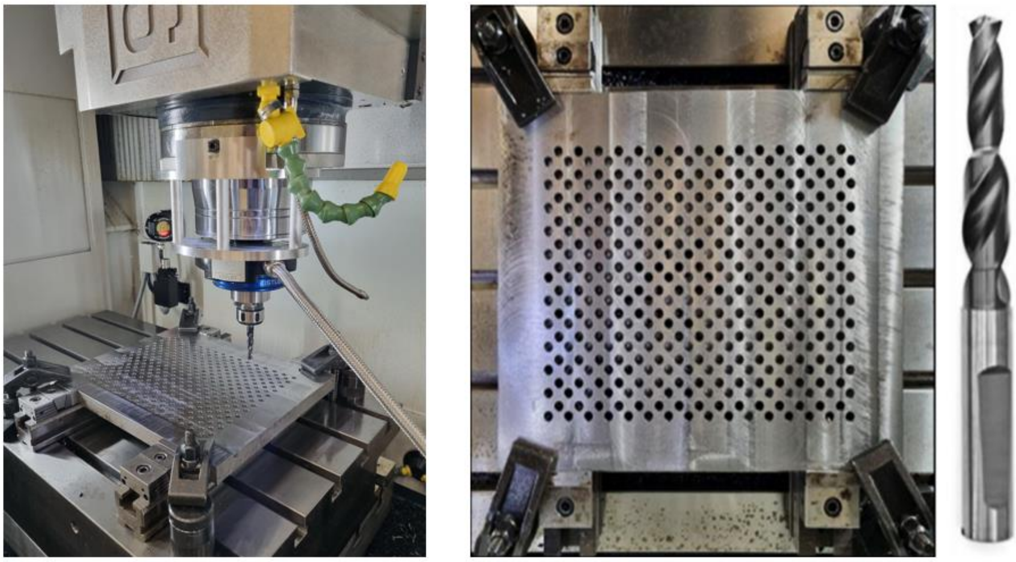

Figure 5.1: Experimental setup for tool wear estimation in drilling with steel workpiece.

The G-code program for the CNC machine tool is programmed such that the cutting tool is drilling 6 rows in a row. For the simplification, drilling of 6 consecutive holes is referred as one set, moreover in the paper. High-frequency actual spindle motor current data collected from Edge and cutting torque data collected from rotary type dynamometer is shown in Figure 5.2. In the figure, the datapoints are representing an increasing trend when the hole number is increasing. Since this trend could be caused by the temperature increase on drill tool margins exerted from friction between steel workpiece and carbide cutting tool, in the next section, temperature analysis will be interpreted.

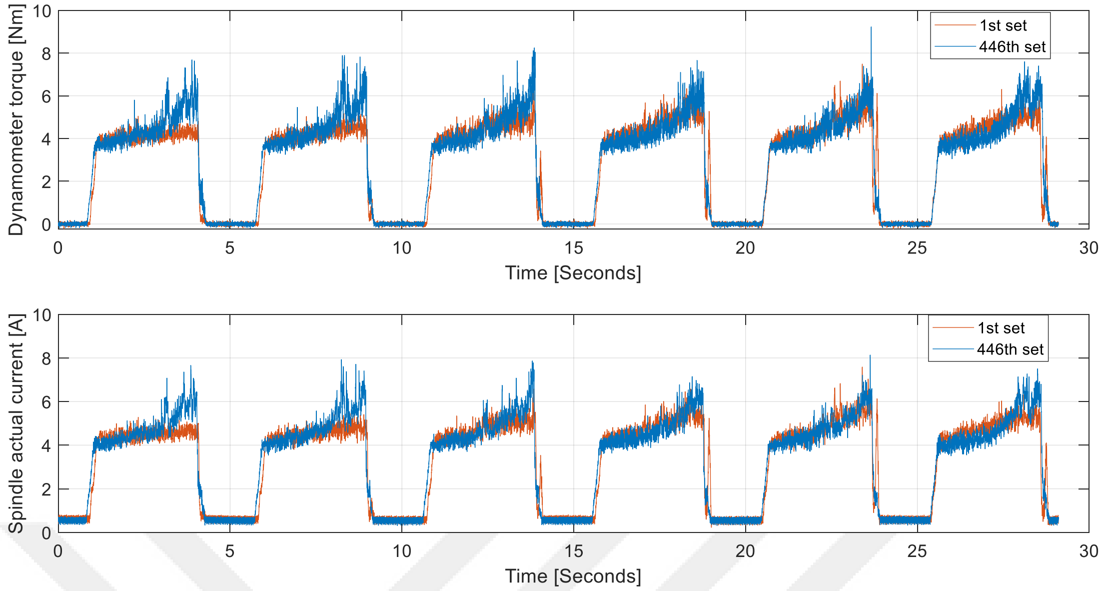

Figure 5.2: Datapoints collected during steel drilling experiments a) cutting torque data collected from rotary type dynamometer b) spindle actual current data collected from Edge.

In Figure 5.3, the mean values during drilling cutting regions are shown for each hole. Also, the moving average of the data constructed from mean values of holes, which has length of 2676 is calculated with 15 window size. Since there is an increasing trend at the last holes of the sets, plotting just mean data of drilled holes can show noisy signals.

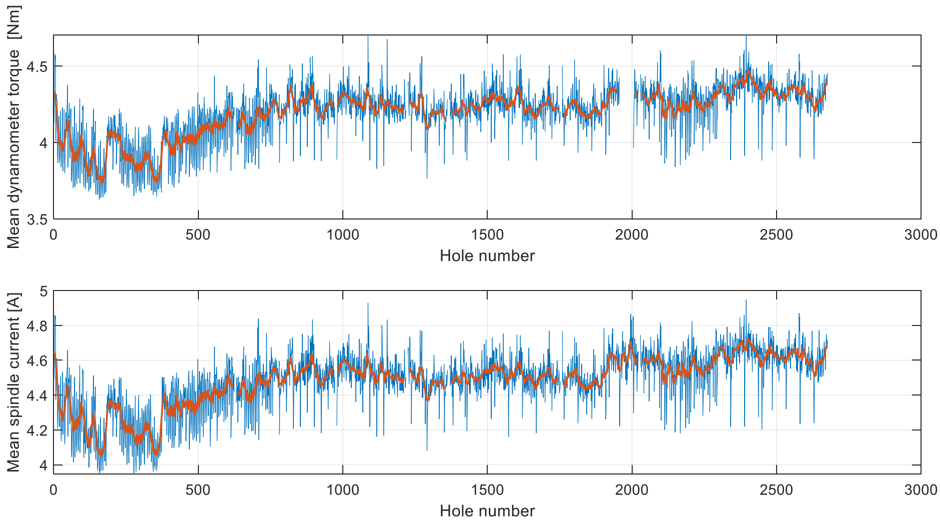

Figure 5.3: Mean values of collected datapoints for each drilled holes and moving averages with 15 window sizes a) mean dynamometer torque values b) mean spindle actual current values.

5.2 *Tool Tip Temperature Analysis*

Tool tip temperature was measured with FLIR thermal camera during machining experiments to inspect tool tip temperature change at consecutive holes. The experimental setup of the camera during steel drilling experiments is shown in Figure 5.4. As it can be seen in Figure 5.4, the camera was placed carefully to inspect the tool tip temperature right after the tool is extracted from the workpiece for 6 consecutive holes. To display camera images and collect data, FLIR software is used. Before starting the experiment, settings for the object on the FLIR software defined such as emissivity (0,95), distance (1,5 m), reflected temperature (25 Celsius), as well as nominal external optics and atmosphere settings. In the software, a rectangular area right above the workpiece to inspect tool tip temperature right after the tool leaves the workpiece. Also, since the consecutive holes are placed on the workpiece vertically, the defined area on the software encapsulates all of 6 holes. The display on the software while drilling first and last hole on the set is shown in Figure 5.4b and Figure 5.4c, respectively.

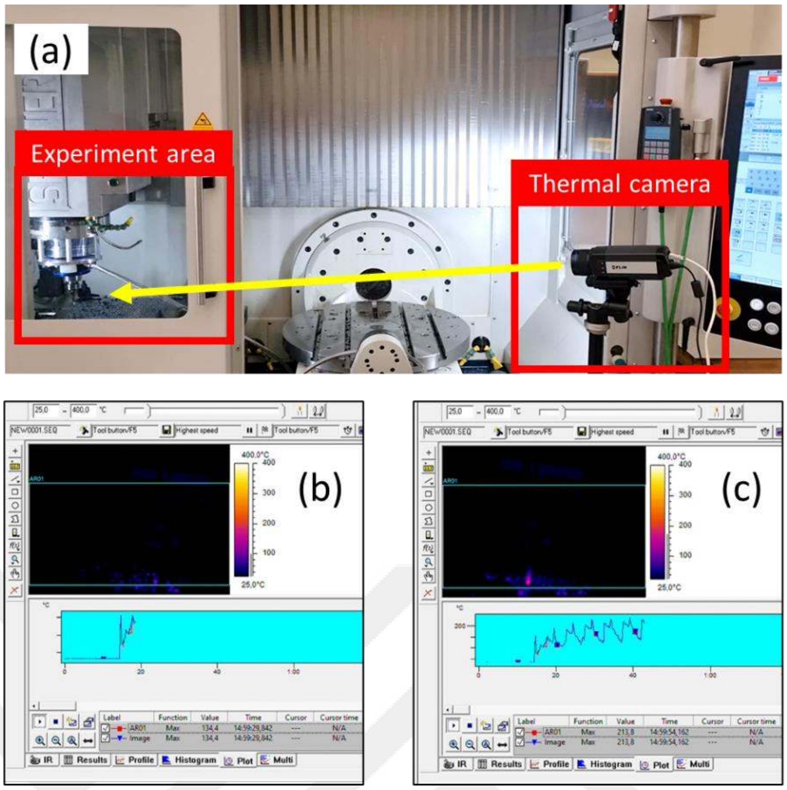

Figure 5.4: Tool tip temperature measurement experiment (a) experimental setup (b) display on measurement software for the first hole in the set (c) display on measurement software for the last hole in the set.

Temperature measurements collected from FLIR software is exported and plotted in MATLAB together with Edge spindle current data to inspect the tool tip temperature differences during drilling 6 consecutive holes. As it shown on Figure 5.5, tool tip temperature increases approximately to 300 Celsius after drilling 6 holes.

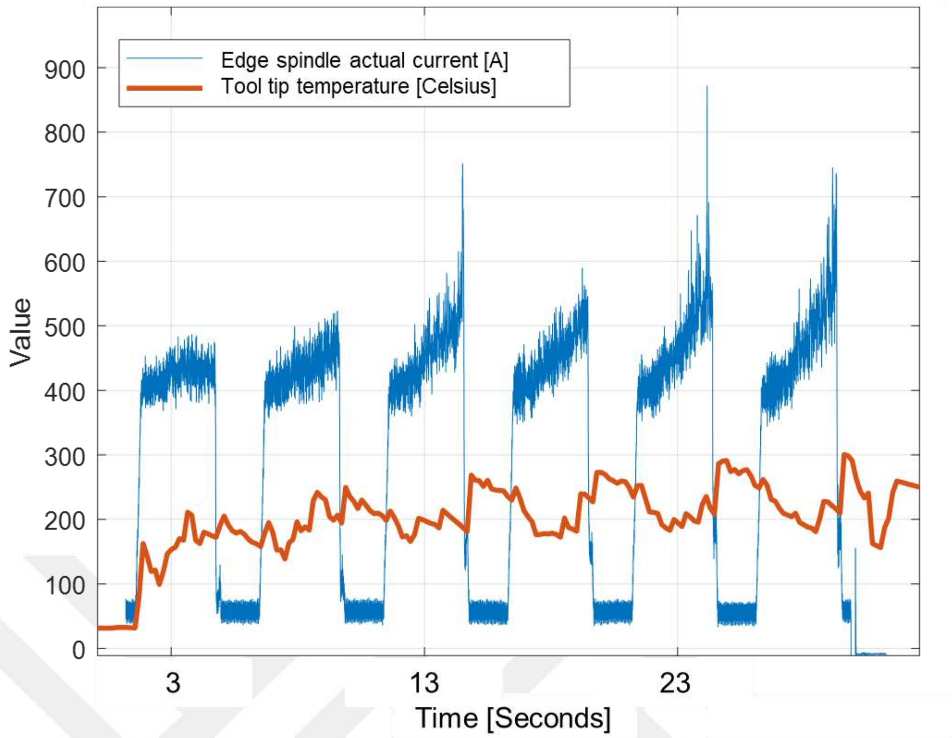

Figure 5.5: Tool tip temperature of drilling 6 consecutive holes on steel plate with Edge spindle actual current signals.

5.3 *Hole Quality*

The position related parameters collected from Edge can also give idea about the quality of the workpiece. In case of drilling, the Edge data can give insights for hole quality. When drilling experiment is conducted in z-axis coordinate, desired value of x-axis and y-axis coordinate positions of servo motor are expected to be constant, so that the diameter of drilled hole will be just equal to the cutting tool's diameter. However, there might be some deviations on the servo motor positions due to friction between workpiece and tool tip or due to other environmental factors and anomalies. To investigate that, the desired positions and encoder positions of x, y and z-axis servo motors during drilling 6 consecutive holes on steel plate are investigated. The deviations are shown in 3-dimensional plot given in Figure 5.6 with normalized values of desired and normalized positions, where the coordinate of the top of the hole is (0,0,0).

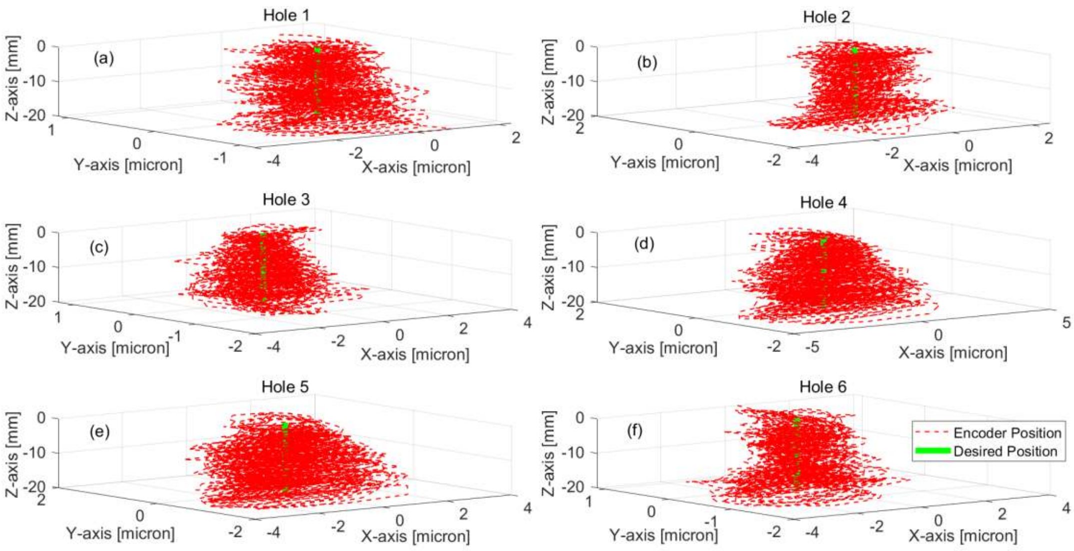

Figure 5.6: 3-dimensional graph for deviations in drilled holes during 6 consecutive drilling of steel workpiece, (a) hole 1, (b) hole 2, (c) hole 3, (d) hole 4, (e) hole 5, (f) hole 6.

The same datapoints are shown in Figure 5.7, Figure 5.8, and Figure 5.9 as well, to inspect the positional deviations within x-z, y-z, and x-y coordinates, respectively.

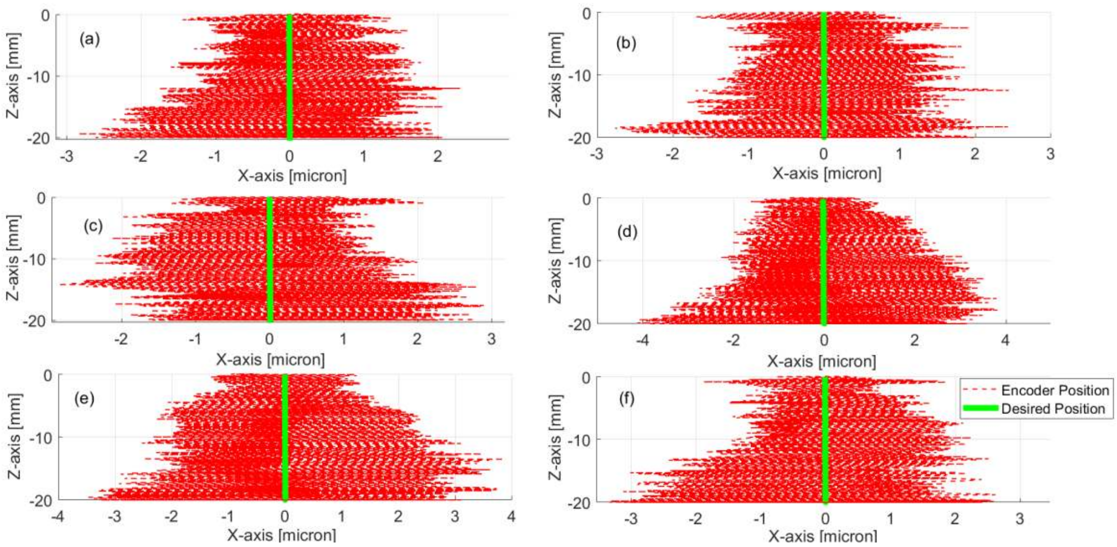

Figure 5.7: X-Z coordinates graph for deviations in drilled holes during 6 consecutive drilling of steel workpiece, (a) hole 1, (b) hole 2, (c) hole 3, (d) hole 4, (e) hole 5, (f) hole 6.

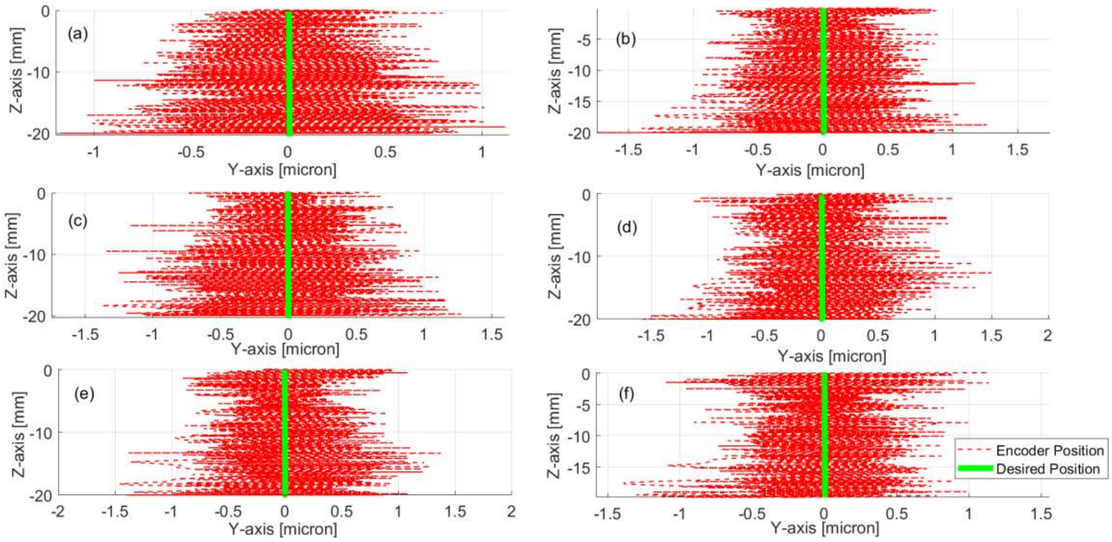

Figure 5.8: Y-Z coordinates graph for deviations in drilled holes during 6 consecutive drilling of steel workpiece, (a) hole 1, (b) hole 2, (c) hole 3, (d) hole 4, (e) hole 5, (f) hole 6.

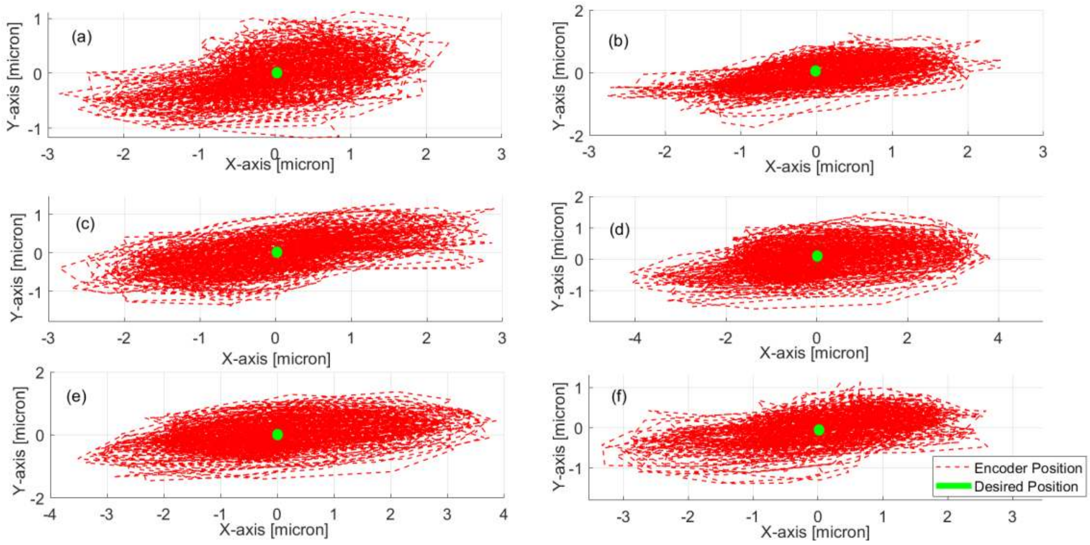

Figure 5.9: X-Y coordinates graph for deviations in drilled holes during 6 consecutive drilling of steel workpiece, (a) hole 1, (b) hole 2, (c) hole 3, (d) hole 4, (e) hole 5, (f) hole 6.

5.4 *Anomaly Detection*

During machining some anomalous conditions can happen from unexpected conditions such as poor material quality of workpiece, sudden torque changes due to friction and breakage of the tool or workpiece, chatter vibrations, poor mounting the workpiece on machine tool plate, poor mounting the cutting tool on tool holder, human error etc. Digital Twin can be developed to monitor these anomalies or predict anomalous conditions with more advanced data or simulation models.

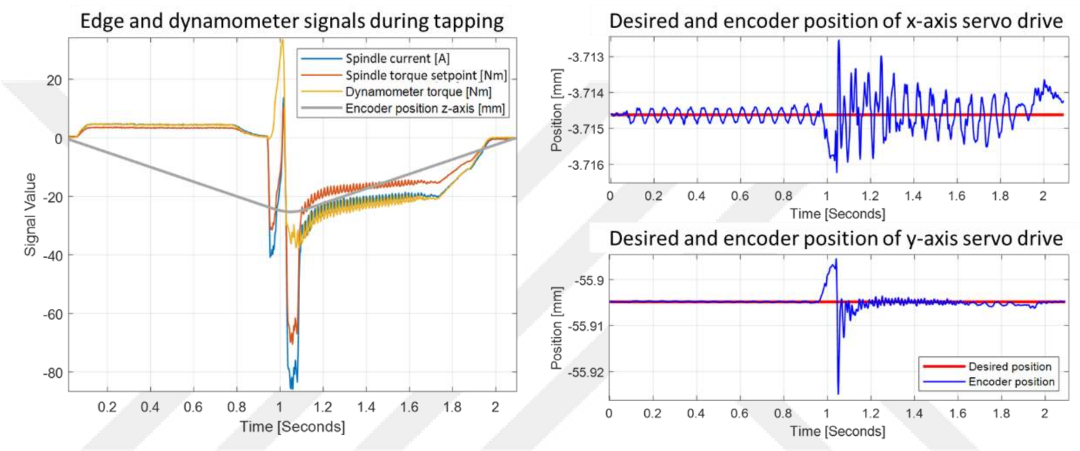

Figure 5.10: Data collected from dynamometer and Edge during anomalous tapping operation.

In Figure 5.10, data collected from Edge device during anomaly of tapping operation. During the experiment, the tapping tool was mounted to the same rotary type dynamometer which shown previously in Figure 3.5. After the experiment, it has been observed that the cutting tool was loosed from dynamometer collet. When the data shown in Figure 5.10 is investigated, according to encoder position in z-axis, when the tapping tool is extracted from the workpiece, fluctuations on dynamometer torque, edge spindle current and encoder positions data is observed. Since the cutting tool needs to turn the opposite way when extracting from workpiece during tapping operation and dynamometer collet is not providing changing on rotation during tapping, the cutting tool is loosed from the dynamometer collet. Such as this example, the data collected from Edge can be fed to real-time time-series models in order to detect and prevent anomalous conditions.

Chapter 6:
CONCLUSION AND FUTURE WORK

In this work, the Edge infrastructure with CNC machine tool was introduced, high-frequency process data collected from Edge was demonstrated and validated with functionalities of closed-loop feed-drive position control and spindle drive current control diagrams for the first time, to provide a foundation for Digital Twin applications with Edge Computing. The block diagrams were validated with collected Edge signals during milling, drilling and air-cut experiments at different spindle speeds. Edge computing was proposed to be utilized with Digital Twin applications in machining since the process data collected from the CNC machine is less expensive compared to sensor data which can require additional setup and tools, also the time-synchronization and latency issues for data acquisition is solved with edge device.

A novel method of cutting torque estimation with real-time Edge signals to replace rotary type dynamometer was proposed in this article. The method is using experimental data to estimate required parameters such as torque constant to be used in mechanical equations. In this work, dynamometer data collected during steel workpiece drilling experiment has taken as ground-truth. The results are validated with drilling experiments with same cutting tool, different workpiece materials and speeds. Prediction errors are calculated for experiments with same steel workpiece as 0.31% and 0.9%, and with cast iron workpiece material as 1.02% and 1.25%. The results show that the model is more precise when applied to same workpiece material.

Different machining Digital Twin use-cases that can be implemented with Edge Computing applications were proposed for future work. Tool wear prediction models can be implemented by using high-frequency internal machine servo drive data collected from Edge device. Tool tip temperature change during drilling 6 consecutive holes on steel workpiece and carbide tool are investigated. The data collected from Edge device is shown together with temperature measurements and the change in trend of Edge device data is visible with tool tip temperature change. These two properties can be linked with data-driven models for the future work. Drilling hole quality is proposed to show with position related data collected from Edge device. Further investigation for workpiece hole quality with Edge Computing applications is proposed. Finally, the Edge Computing applications can used within Digital Twin applications that provides anomaly detection. An anomalous tapping experiment is investigated with spindle current, spindle torque setpoint, drive encoder position and desired position data.

REFERENCES

[1] Vaidya, S., Ambad, P., & Bhosle, S. (2018). Industry 4.0 – A Glimpse. Procedia Manufacturing. 20:233-238.

[2] Ghobakhloo, M. (2018). The future of manufacturing industry: a strategic roadmap toward Industry 4.0. Journal of Manufacturing Technology Management. 29(6):910–936.

[3] Rossit, D. A., Tohmé, F., & Frutos, M. (2019). A data-driven scheduling approach to smart manufacturing. Journal of Industrial Information Integration. 15:69–79.

[4] Namjoshi, J., & Rawat, M. (2022). Role of smart manufacturing in industry 4.0. Materials Today: Proceedings. 63:475–478.

[5] Morgan, J., Halton, M., Qiao, Y., & Breslin, J. G. (2021). Industry 4.0 smart reconfigurable manufacturing machines. Journal of Manufacturing Systems. 59:481–506.

[6] Kritzinger, W., Karner, M., Traar, G., Henjes, J., & Sihn, W. (2018). Digital Twin in manufacturing: A categorical literature review and classification. IFAC-PapersOnLine. 51(11):1016–1022.

[7] Tao, F., Qi, Q., Wang, L., & Nee, A. Y. C. (2019). Digital Twins and Cyber–Physical Systems toward Smart Manufacturing and Industry 4.0: Correlation and Comparison. Engineering. 5(4):653–661.

[8] Tao, F., Cheng, J., Qi, Q., Zhang, M., Zhang, H., & Sui, F. (2017). Digital twin-driven product design, manufacturing and service with big data. The International Journal of Advanced Manufacturing Technology. 94(9–12):3563–3576.

[9] Huang, Z., Wiesch, M., Fey, M., & Brecher, C. (2022). Edge computing-based virtual measuring machine for process-parallel prediction of workpiece quality in metal cutting. Procedia CIRP. 107:363–368.

[10] Liu, B., Zhang, Y., Zhang, G., & Zheng, P. (2019). Edge-cloud orchestration driven industrial smart product-service systems solution design based on CPS and IIoT. Advanced Engineering Informatics. 42:100984.

[11] Liu, S., Lu, Y., Zheng, P., Shen, H., & Bao, J. (2022). Adaptive reconstruction of digital twins for machining systems: A transfer learning approach. Robotics and Computer-Integrated Manufacturing. 78:102390.

[12] Bilgili, D., Kecibas, G., Besirova, C. et. al. (2023). Tool flank wear prediction using high-frequency machine data from industrial edge device. Procedia CIRP, 118, 483–488.

[13] Ghosh, A. K., Ullah, A. S., Teti, R., & Kubo, A. (2021). Developing sensor signal-based digital twins for intelligent machine tools. Journal of Industrial Information Integration. 24:100242.

[14] Korkmaz, M. E., Gupta, M. K., Li, Z. et al (2022). Indirect monitoring of machining characteristics via advanced sensor systems: a critical review. The International Journal of Advanced Manufacturing Technology. 120(11–12):7043–7078.

[15] Mohanraj, T., Shankar, S., Rajasekar, R. et al (2020). Tool condition monitoring techniques in milling process — a review. Journal of Materials Research and Technology. 9(1):1032–1042.

[16] Beşirova C, Akhtar W, Shahzad A. et al. Analysis of Machining Process with Data Collection Using Industrial Edge Computing. 11th International Congress on Machining, Istanbul: 2021.

[17] Altintas, Y. (2012). Manufacturing Automation. Cambridge University Press.

[18] Xu, G., Zhou, H., & Chen, J. (2018). CNC internal data based incremental cost-sensitive support vector machine method for tool breakage monitoring in end milling. Engineering Applications of Artificial Intelligence. 74:90–103.

[19] Siemens (2011) SINUMERIK 840D sl / 828D Basic Functions: Function Manual.

[20] Altintas, Y., Yang, J., & Kilic, Z. M. (2019). Virtual prediction and constraint of contour errors induced by cutting force disturbances on multi-axis CNC machine tools. CIRP Annals. 68(1):377–380.

[21] Fertig, A., Weigold, M., & Chen, Y. (2022). Machine Learning based quality prediction for milling processes using internal machine tool data. Advances in Industrial and Manufacturing Engineering. 4:100074.

[22] Aslan, D., & Altintas, Y. (2018). On-line chatter detection in milling using drive motor current commands extracted from CNC. International Journal of Machine Tools and Manufacture. 132:64–80.

[23] Aslan, D., & Altintas, Y. (2018). Prediction of Cutting Forces in Five-Axis Milling Using Feed Drive Current Measurements. IEEE/ASME Transactions on Mechatronics, 23(2):833-844.

[24] Altintas, Y., & Aslan, D. (2017). Integration of virtual and on-line machining process control and monitoring. CIRP Annals. 66(1):349–352.

[25] Miao, H., Wang, C., Hao, J. et al (2022). Dynamic analysis of the column-spindle system considering the nonlinear characteristics of kinematic joints. Mechanism and Machine Theory. 174:104922.

[26] Suh S-H, Kang SK, Chung D-H, Stroud I (2008) Theory and design of CNC systems. Springer London.

[27] Siemens (2012) SINUMERIK 840D sl CNC Commissioning: NCK, PLC, drive: Commissioning Manual.

[28] Siemens (2021) SINUMERIK EDGE: Programming Manual.

[29] Siemens (2014) SINAMICS SINAMICS S120/S150: List Manual.

[30] Siemens (2018) SINUMERIK 840D sl Extended Functions: Function Manual.

[31] Zhou, K., Ai, M., Sun, D. et al (2019). Field Weakening Operation Control Strategies of PMSM Based on Feedback Linearization. Energies. 12(23):4526).

[32] Kumar, R., & Murmu, R. (2020). Performance Analysis of Permanent Magnet Synchronous Motor. International Journal of Engineering Research & Technology (IJERT), NCSMSD - 2020 Conference Proceedings, Special Issue - 2020. ISSN: 2278-0181.

[33] Kefsi, L., Touzani, Y., & Gabsi, M. (2010). Hybrid Excitation Synchronous Motor control with a new flux weakening strategy. 2010 IEEE Vehicle Power and Propulsion Conference, 1-5.

[34] Xu, L., Ye, L., Zhen, L., & El-Antably, A. (1995). A new design concept of permanent magnet machine for flux weakening operation. IEEE Transactions on Industry Applications, 31(2):373–378.

[35] Stumberger, B., Hamler, A., Trlep, M., & Jesenik, M. (2001). Analysis of interior permanent magnet synchronous motor designed for flux weakening operation. IEEE Transactions on Magnetics, 37(5):3644–3647.